Results in Engineering 16 (2022) 100737

Contents lists available at ScienceDirect

Results in Engineering

journal homepage: www.sciencedirect.com/journal/results-in-engineering

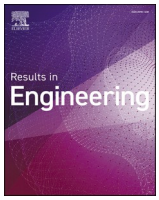

Pd supported on defective TiO_2 polymorphic mixtures: Effect of metal-support interactions upon glycerol selective oxidation

Matías Gastón Rinaudo [a,*], Ana María Beltrán [b], Asunción Fernández [c], Luis Eduardo Cadús [a], Maria Roxana Morales [a]

[a] Instituto de Investigaciones en Tecnología Química (INTEQUI-CONICET), Universidad Nacional de San Luis (UNSL), Facultad de Química Bioquímica y Farmacia, Almirante Brown 1455, Capital, 5700, San Luis, Argentina
[b] Departamento de Ingeniería y Ciencia de los Materiales y del Transporte, Escuela Politécnica Superior, Universidad de Sevilla, Virgen de África 7, 41011, Sevilla, Spain
[c] Instituto de Ciencia de Materiales de Sevilla, (CSIC-Univ. Sevilla), Avda. Américo Vespucio 49, 41092, Sevilla, Spain

ARTICLE INFO

Keywords:
Titanium oxide polymorphs
Glycerol selective oxidation
Palladium-based catalyst
Metal-support interaction
Mechanochemical activation

ABSTRACT

Palladium catalysts supported on defective mixes of anatase, TiO_2 (II) and rutile crystalline phases, previously obtained by high-energy ball milling, were synthesized and tested for glycerol selective oxidation. A deep characterization of these unusual materials was carried out to elucidate catalytic and physicochemical features. Electron density transfer from support to metal or vice versa, depending on the polymorphs present, could not only alter palladium particle sizes and its surface oxidation state but also reducibility and oxygen mobility of catalysts. Furthermore, acid-base properties achieved also influenced catalytic activity under mild conditions of liquid-phase glycerol oxidation. A conversion of 94% and a selectivity to glyceric and lactic acids of 48% and 22% respectively were obtained for the Pd catalyst supported on mechanochemically activated anatase. The presence of several polymorphs in a metal oxide support could therefore benefit or handicap catalytic cycle for a particular reaction. Metal-support interactions play a key role in heterogenous catalysts and thus the rational design of supports comes on the scene.

1. Introduction

With the actual trend to biomass-based fuels, valorization of by-products obtained in these processes becomes an interesting alternative to promote green and sustainable technologies [1,2]. In case of biodiesel, direct substitute of diesel, the increasing demand observed in the last years is also accompanied by raw glycerol as a surplus by-product (obtained in order of 10 wt%). This situation leads to the need of glycerol conversion into value-added products, to increase carbon balance and improve the economy of biodiesel production [3,4]. Fortunately, the renewable nature and high-functionality of glycerol has attracted the interest of scientific community in its transformation [3,5,6]. Among different routes, glycerol selective oxidation is an attractive alternative due to low-cost, availability and eco-friendly origin of air or oxygen used as co-reactant, giving expensive oxygenated products such as dihydroxyacetone, glyceric and lactic acids as products [4,7–9]. Glyceric acid is currently used as platform to produce amino acids such as serine but also to treat skincare disorders due to its proven biological activity [10]. In case of lactic acid, it is widely used in different areas including food, pharmaceutical and textile industries [2]. However, its most significant application is as precursor for the production of polylactic acid, which is considered as one of the most promising bioplastics to substitute petroleum-derived plastics such as polystyrene, polypropylene, and polyethylene terephthalate [11]. Liquid-phase glycerol selective oxidation under basic conditions and using supported catalysts includes a complex reaction network (Scheme 1) that involves several pathways to obtain corresponding aldehyde, ketone and carboxylic acids [8,9]. As stated in the literature, a high pH commonly achieved by NaOH addition is needed for the initial deprotonation of glycerol and further dehydrogenation to glyceraldehyde and/or dihydroxyacetone, followed by oxidation to acid products [3,8,12]. Among different steps in both solution and over catalyst's surface, several authors agreed that oxygen is indirectly involved during oxidation, removing electrons from the surface and regenerating hydroxyl groups to close catalytic cycle [8,12,13]. Accordingly, to achieve good conversion and selectivity, the selection of an active phase and support gains great relevance. In this matter, mono and bimetallic catalysts based on Pd, Pt and Au supported on different metal oxides and carbon materials have been extensively

* Corresponding author.
E-mail address: matirinaudo@gmail.com (M.G. Rinaudo).

https://doi.org/10.1016/j.rineng.2022.100737
Received 16 August 2022; Received in revised form 15 October 2022; Accepted 28 October 2022
Available online 31 October 2022

used in liquid-phase oxidation reactions, where both dispersion and particle size of metal particles are considered to be the dominant factors for a good activity and selectivity [14,15]. However, the role of supports is not limited to act as metal particles carriers [16–18]. Several times, the interface between metal and support becomes a better active site than the metal itself and thus, an appropriate selection of a catalyst support could reduce the quantity of expensive metals needed (e.g. noble metals) [3,15,16,19–21]. In case of glycerol oxidation, metal oxides with redox properties are known to have higher mobility of adsorbed hydroxyl and oxygen species at the interface between metal and support [8]. Moreover, metal-support interaction is a well-known phenomenon attributed to electronic and geometric effects that induce charge transfer between metal particles and support [15,19,22]. These interactions together with acid-base nature of support might not only enhance the adsorption capacity of active sites but also inhibit the sintering of metal particles during oxidation [3,17,23]. A shortcoming remains in the literature when it comes to understanding support's contribution on catalytic performance, e.g. when defective metal oxides and different polymorphs are present in a given support. A rational design including the support is therefore crucial to obtain sustainable metal-supported catalyst with high activity, reusability and selectivity to desired products [16,22,24,25].

Considering several metal oxides, TiO_2 is a recognized support for metals which shows different properties depending on the polymorphs present in its structure [16]. Since most reactions in heterogeneous catalysis take place on the surface of metal active phase and/or boundaries between metal and support, the presence of various crystalline phases could impact on catalytic properties [15,16,26]. To the best of our knowledge, catalysts with modified TiO_2 supports formed by defective structures and unusual polymorphic mixtures have not been used for glycerol selective oxidation until now. Hence, we propose the study of palladium catalysts supported on mixes of anatase, TiO_2 (II) and rutile phases obtained by high-energy ball milling in a previous work [27] to evaluate the role of their different physicochemical properties and metal-support interactions in liquid-phase glycerol selective oxidation.

2. Experimental

2.1. Catalysts preparation

Wet impregnation method was used to deposit palladium on three different TiO_2 supports obtained in a previous work [27]. 2 mL of a 0.1 M aqueous solution of HCl (37.0 wt%, Anedra) with appropriate quantities of $PdCl_2$ (99.9%, Sigma Aldrich) was added to each titania support in order to achieve palladium loadings of 0.25 wt% on a metal basis. Recovered solids were dried in an oven under vacuum at 70 °C overnight. Then, samples were calcined in a muffle furnace under air at 500 °C for 4 h using a heating ramp of 10 °C min^{-1} to eliminate the rests of metal precursor. Final Pd supported catalysts were labeled **Pd/Ti$_x$**

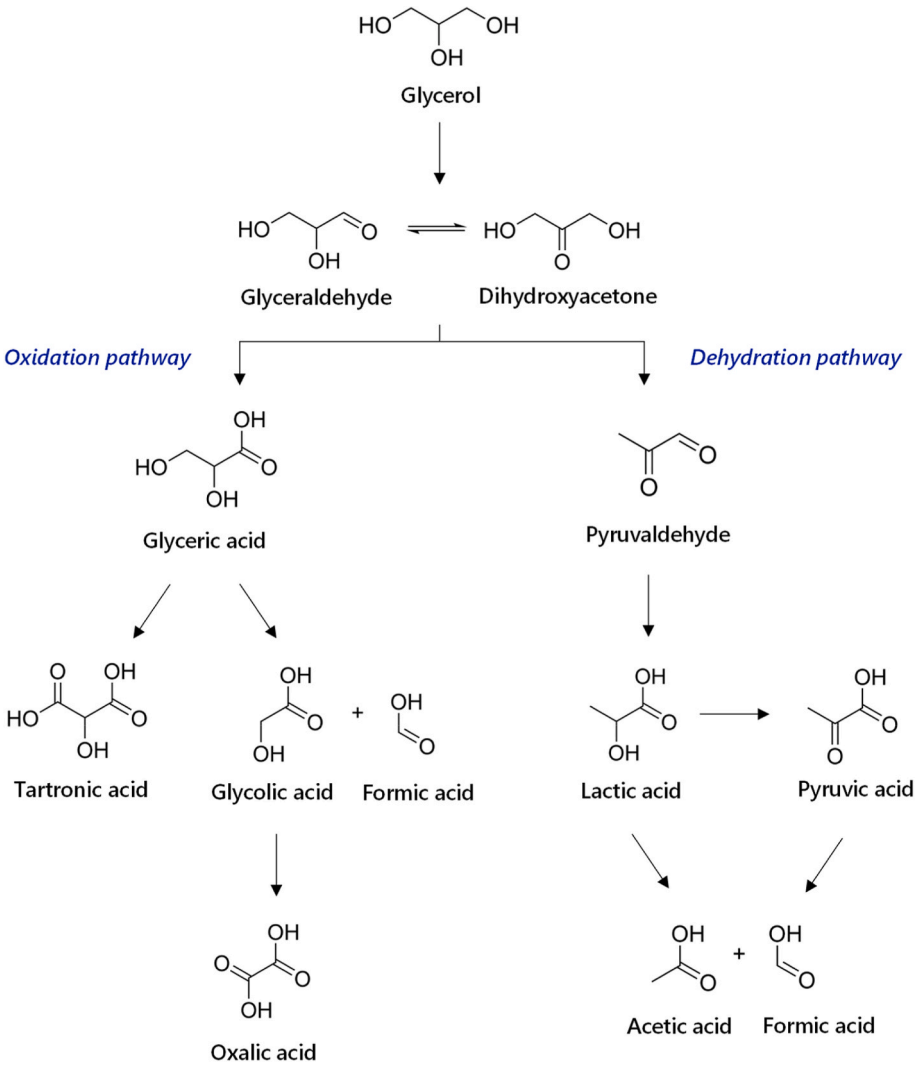

Scheme 1. Reaction network for glycerol oxidation.

where x corresponds to the milling time of previously synthesized supports.

2.2. Characterization

2.2.1. X-ray diffraction (XRD)

X-ray diffraction was performed using a Rigaku Ultima IV diffractometer operated at 20 mA and 30 kV with a Cu Kα ($\lambda = 0.15405$ nm) radiation lamp. Step scan data were recorded at a step width of 0.02° and a counting time of 2 s.

2.2.2. Raman spectroscopy

Raman spectroscopy was carried out using an Ar^+ laser excitation (514 nm) varying the source power and a resolution of 3 cm^{-1} (Model RAMAN-Renishaw - Invia Raman Microscopy).

2.2.3. Scanning electron microscopy (SEM-EDX)

Morphology of the catalysts was studied with a scanning electron microscope coupled to Electron Dispersive X-ray Spectroscopy system (LEO 1450 VP SEM). Samples were deposited on aluminum sample holders and sputtered with gold before analysis.

2.2.4. Transmission Electron Microscopy (TEM)

Transmission Electron Microscopy (TEM) studies were performed in a FEI TALOS F200S microscope operating at an accelerating voltage of 200 kV. For TEM analyses, samples were dispersed in ethanol by ultrasound before dropping them in a holey carbon film on a copper grid. Samples were studied by High-Angle Annular Dark-Field (HAADF) imaging, Scanning Transmission Electron Microscopy (STEM) and Energy-dispersive X-ray Spectroscopy (EDS).

2.2.5. Textural analyses

Textural properties were evaluated by Brunauer-Emmet-Teller (BET) method using nitrogen adsorption at 77 K in a Micromeritics Gemini V equipment. Catalysts were previously outgassed overnight at 250 °C under N_2.

2.2.6. Inductively coupled plasma – optical emission spectroscopy (ICP-OES)

Pd content was checked in an ICP- Varian-Ashilet equipment after digestion of the catalysts in a mixture of HNO_3, HCl and HF acids.

2.2.7. X-ray photoelectron spectroscopy (XPS)

XPS spectra were recorded with a SPECS Multitechnique instrument equipped with a dual X-ray source of Mg/Al and a PHOIBOS 150 hemispheric analyzer. A pass energy of 30 eV and an Al anode operated at 200 W was used. The pressure was kept under 1×10^{-9} mbar during all measurements. Spectra were obtained for the C 1s, O 1s, Ti 2p and Pd 3 d regions. C 1s binding energy (284.6 eV) was used as internal reference to correct peak positions. XPSPeak 4.1 free software was used for data processing.

2.2.8. Temperature programmed measurements

H_2-Temperature Programmed Reduction (H_2-TPR) and O_2-Temperature Programmed Desorption (O_2-TPD) were carried out in a home-made equipment using a quartz tubular reactor and a TCD detector under the same conditions reported in a previous study [27].

2.2.9. 2-Propanol decomposition test

Acid-base properties were studied through 2-propanol decomposition test in a fixed-bed stainless-steel tubular reactor. 50 mg of each catalyst and support, with particle sizes between 300 and 600 μm, were firstly pretreated in Ar (150 mL min^{-1}) for 30 min at 290 °C and atmospheric pressure. Reaction tests were performed introducing 7.5 vol % isopropanol (99.5%, Sintorgan) to the reactor, using Ar as carrier and the same operational conditions for 120 min. Products were analyzed in an online gas chromatograph (Buck Scientific 910) equipped with an FID detector and a silica capillary GC column (SPB1).

2.3. Catalytic tests

2.3.1. Reaction conditions

Glycerol selective oxidation was carried out in a 50-mL steel Parr type reactor equipped with a pressure gauge, oven and controllers for temperature and agitation. 20 mL of 0.15 M glycerol (99.7%, Biopack) aqueous solution, sodium hydroxide (≥97.0%, Biopack) to reach NaOH: glycerol molar ratio of 2 and 200 mg of catalyst (glycerol:Pd theoretical molar ratio of 600) were added into the reactor. Mixture was heated to 100 °C under 1000 rpm of agitation speed and 1 bar of pure oxygen for 4 h.

2.3.2. Products analyses

Products analyses were performed in an HPLC equipped with an Aminex HPX-87H column (300 × 7.8 mm) and an UV diodes array as detector. A 0.005 M solution of H_2SO_4 (98.0%, Anedra) was used as eluent at 30 °C and a flow rate of 0.6 mL min^{-1}. Identification and quantification of products was carried out by comparison with external calibration curves using standard solutions of each chemical: glycerol (99.7%, Biopack); lactic acid (Pharmaceutical Secondary Standard, Merck), D-glyceric acid sodium salt (≥95.0%, Merck); oxalic acid (99.5%, Ucb); formic acid (85.0%, Thermo Scientific). An aliquot of each reaction sample was firstly filtered and neutralized by adding a fixed quantity of H_2SO_4 solution before chromatographic analysis.

3. Results and discussion

Materials presented herein consist of a complex matrix that includes palladium particles and different arrangements of TiO_2 polymorphs with defective structures induced by ball-milling. An exhaustive characterization is therefore required to comprehend its properties and how they could impact on catalytic behavior.

3.1. XRD analyses

It is known that the nature of supports can highly affect the shape and dispersion of active species, improving the stability of catalysts during reaction [16,28]. Hence, XRD analyses were performed to evaluate the crystalline structure of supported catalysts. We observed (Fig. 1 A) that samples were formed by different mixtures of titania polymorphs. Pd/Ti5 showed intense reflections associated to anatase phase (PDF 00-21-1272) but also two broad and low-intensity reflections at angles of 27.54° and 31.53° attributed to (110) rutile reflection (PDF 00-21-1276) and (111) high-pressure TiO_2 (II) reflection (PDF 00-72-0021) respectively. These observations confirmed the presence of an almost pure anatase phase in this catalyst, as expected for its support [27]. On the other hand, Pd/Ti45 exhibited an increase in both TiO_2 (II) and rutile reflections but a decrease in anatase reflections. Pd/Ti120 also showed the reflection attributed to TiO_2 (II) phase and the appearance of several high-intensity rutile reflections. Obtained results revealed the different composition of titania phases present in the three catalysts. Furthermore, broad signals observed were expected due to lattice defects and small particles present in milled supports [29]. Palladium content of catalysts (0.25 wt%) could be considered out of the detection limits of XRD equipment [26]. However, an incipient signal of (101) PdO reflection (PDF 00-06-0515) at 34.04° was detected in Pd/Ti5 catalyst. This behavior suggested the presence of larger palladium particles deposited on this catalyst, also supported by a further TEM analysis. In addition, oxidized species of palladium were likely to be formed since all catalysts were calcined in air at 500 °C [30]. The absence of this signal in Pd/Ti45 and Pd/Ti120 catalysts could be associated to smaller particles finely dispersed on the supports, favored by the greater number of defects and the combination of polymorphs present in these supports

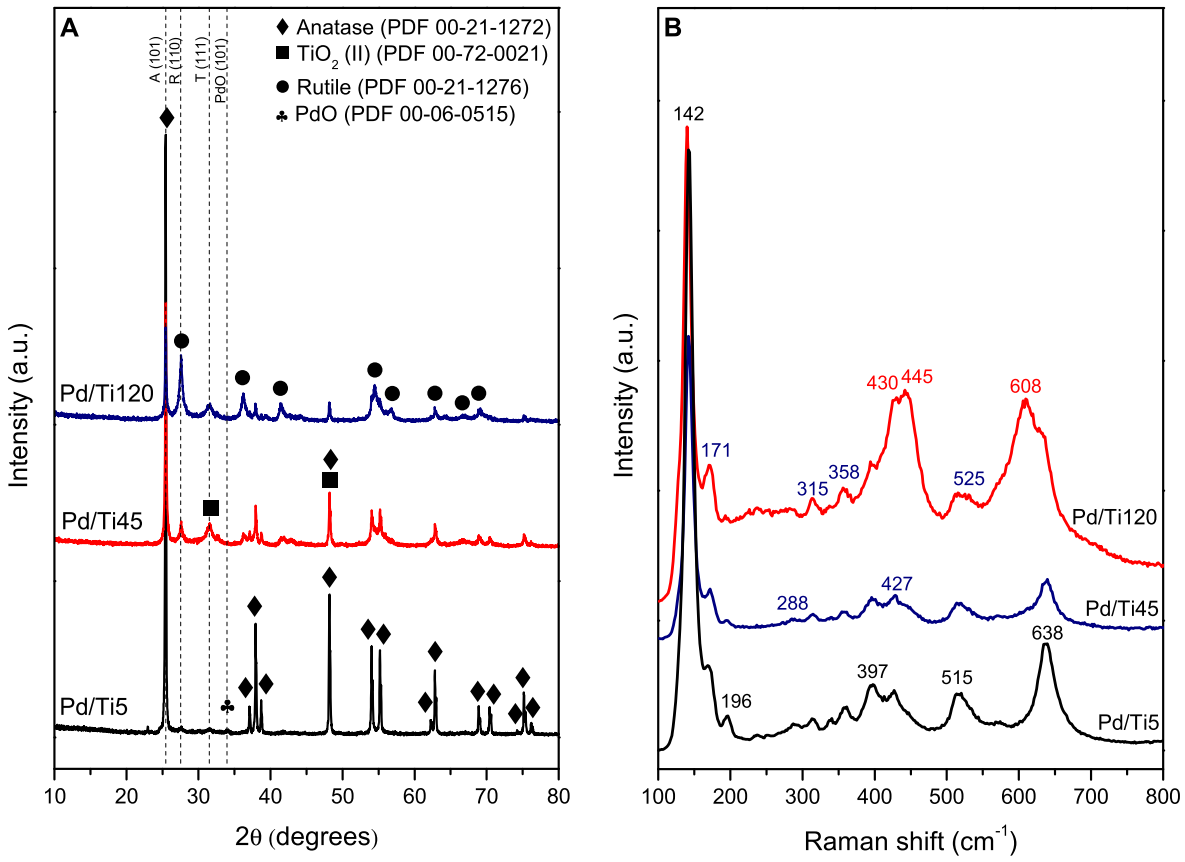

Fig. 1. XRD spectra (A) and Raman spectra (B) of catalysts.

[25,27,30–32].

We also made a rough calculation of average crystallite sizes of the catalysts by means of Scherrer equation and the relative intensities of the most intense reflection of each crystalline phase, (101) anatase, (110) rutile and (111) TiO_2 (II), as suggested by Dulian et al. [33]. We observed (Table 1) a reduction trend according to supports' milling extent and the particle refinement caused by mechanochemical process [27,34]. These results were also in line with the increase in S_{BET} values (Table 1) observed in a subsequent analysis. We found smaller crystallite sizes for Pd/Ti5 and Pd/Ti45 compared to the values obtained for respective supports (66 and 49 nm respectively) [27]. This fact was associated to the combined effect of acid medium during preparation, palladium deposition and calcination at 500 °C which could modify titania structures. Being anatase the main phase present in both catalysts, less stable particles of support may be deagglomerated and re-crystalized during synthesis steps. In case of Pd/Ti120, the crystallite size increased compared to the support (23 nm), showing more intense reflections, which could be associated to the stability of rutile and crystal growth during calcination [27]. We also estimated the catalysts composition (Table 1) using the most intense Bragg reflection of each titania phase and the equations reported by Duvarci et al. [35,36]. Results showed the unusual mixes of titania phases present in the supports [27] with greater quantity of anatase phase in case of Pd/Ti45 and more evidently in Pd/Ti120. These results could be associated to palladium addition and further calcination, which is known to stabilize anatase phase, as reported by other authors [37]. Moreover, formation of stable intermetallic structures between Ti from anatase and palladium could induce a reverse transformation from TiO_2 (II) and/or rutile to anatase, increasing the quantity of the latter [37].

Even though the mixture of crystalline structures and impurities is a drawback when using mechanochemical and thermal steps of synthesis, the existence of grain boundaries between different phases of titania could not only benefit charge mobility but also serve as energetic sites for reactants and/or products, improving the catalytic cycle during reaction [38].

3.2. Raman, morphological and textural analyses

Raman spectroscopy (Fig. 1 B) was performed to sustain the results from XRD. High-intensity bands observed at 142, 397, 515 and 638 cm^{-1} were attributed to anatase phase while bands at 171, 315, 427 and 525 cm^{-1} were associated to TiO_2 (II) phase [27,39,40]. Additionally, signals observed at 430, 445 and 608 cm^{-1} were related to rutile phase [41,42]. Once again, Raman results also confirmed titania phases present in the catalysts, with no evidence of palladium species due to its low concentration and/or high dispersion.

Table 1
Weight fraction (%) of titania polymorphs, average crystallite size and textural properties of the catalysts.

Catalyst	Anatase wt%	TiO_2 (II) wt%	Rutile wt%	Average crystallite size (nm)	S_{BET} ($m^2\ g^{-1}$)	Pore diameter (nm)[a]	Total Pore Volume ($cm^3\ g^{-1}$)[b]
Pd/Ti5	99.2	0.3	0.5	54.2	10.0	20.9	0.05
Pd/Ti45	48.4	43.3	8.3	44.1	15.3	26.0	0.10
Pd/Ti120	23.0	49.4	27.6	42.1	17.2	8.8	0.04

[a] BJH adsorption branch average pore diameter.
[b] Quantity of N_2 adsorbed at relative pressure of 0.98.

Textural and morphological properties are also important to understand catalysts' surface architecture. From textural analyses, we observed specific surface area (S_{BET}) values (Table 1) in accordance with the milling time of each titania support. Considering the measurement error of ± 1 m^2 g^{-1}, values were in the order of the ones obtained for the supports [27] even after palladium addition and calcination. These results might indicate that neither the small quantity of palladium nor the synthesis conditions blocked and/or collapsed supports' pores [15]. It is worth highlighting that surface areas obtained were lower than typical values for metals supported on oxides (at least 50 m^2 g^{-1}). However, these values were adequate enough to disperse small quantities of palladium (0.25 wt%), as observed by STEM following analyses. Pore diameters varied in the range 9–21 nm (Table 1) with slightly higher values in case of Pd/Ti5 and Pd/Ti45 compared to the supports [27]. This could indicate that pores' morphology changed at some extent during catalysts synthesis, particularly in the case of supports with greater quantity of anatase phase, and in line with previous XRD discussion [43,44]. Additionally, total pore volumes located in the range 0.04–0.1 cm^3 g^{-1} (Table 1) as expected for the low porosity of titania [26,40]. These values were also higher than respective ones for Pd/Ti5

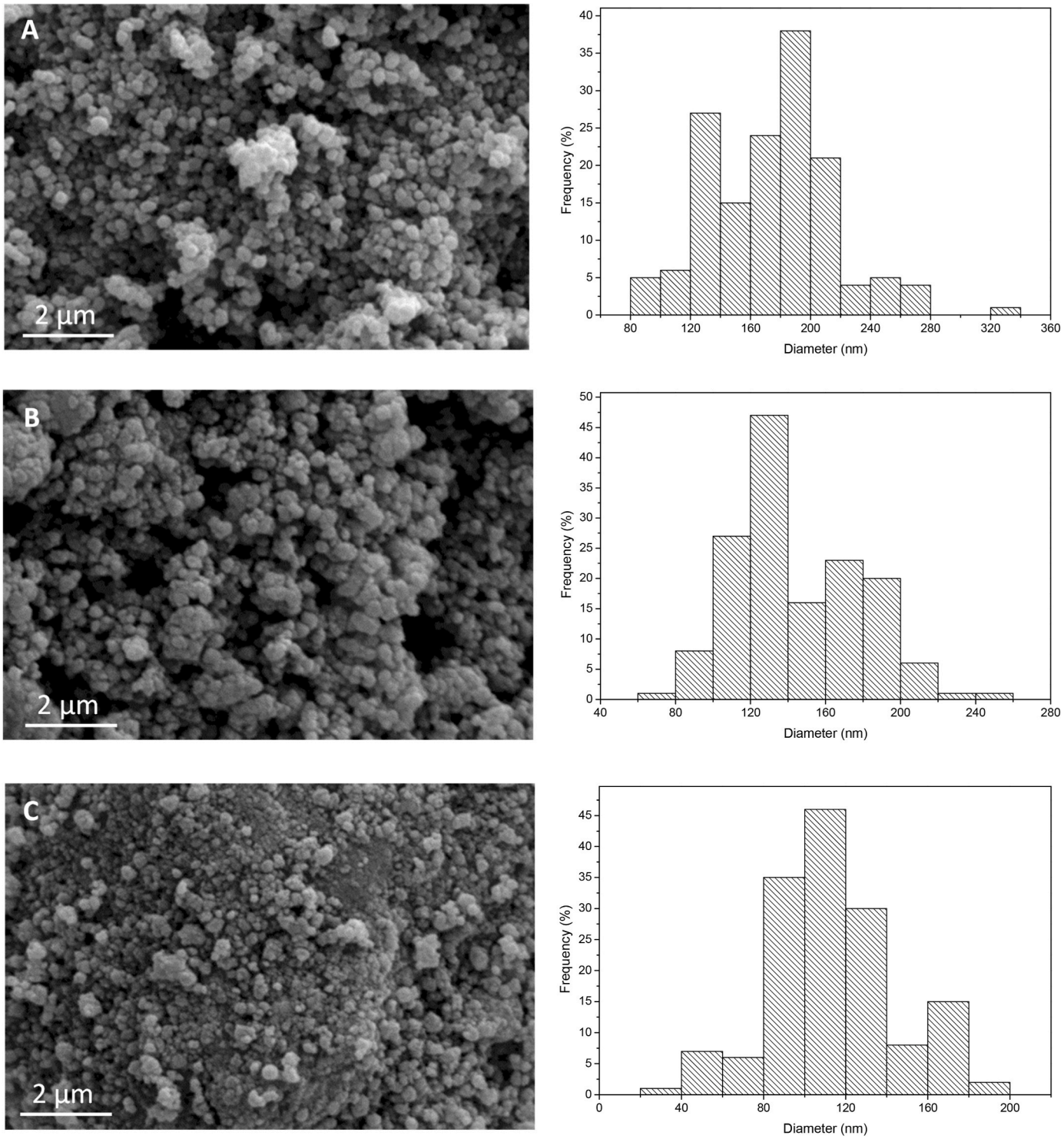

Fig. 2. SEM micrographs (10 kx) and Particle Size Distribution (PSD) histograms of catalysts: Pd/Ti5 (A), Pd/Ti45 (B) and Pd/Ti120 (C).

and Pd/Ti45 supports, which could also be attributed to the catalysts preparation [44]. In spite of these changes, S_{BET} values were not affected. It is important to notice that pore sizes obtained were higher enough to transport big reactant molecules, such as glycerol (average molecule size of 0.62 nm) and hence reaction rate decrease due to internal diffusion is improbable to happen [3,45]. Furthermore, low porosities observed may indicate that S_{BET} values corresponded almost entirely to the external surface area [3], which could induce the preferential location of palladium species on external surface of supports, favoring the access of reactants to start the mechanism of reaction [3].

Morphology of catalysts was studied by SEM. Pd/Ti5 sample (Fig. 2 A) showed particles with spherical shape and diameters between 120 and 220 nm. Pd/Ti45 catalyst (Fig. 2 B) presented grape-like clusters formed by a couple of particles, with average diameters between 100 and 200 [46]. These agglomeration might be a consequence of electrostatic effect on fine particles (with increased surface energy) as reported by other authors [46,47]. Smaller sizes were observed in case of Pd/Ti120 (Fig. 2C) within a range of 80–180 nm. Results were in line with the ones observed for the supports, with a reduction in particle sizes when increasing milling time [27]. Moreover, the smaller particle sizes correlated well with the increase in S_{BET} values (Table 1) from Pd/Ti5 to Pd/Ti120.

3.3. ICP-OES and STEM-EDS analyses

Pd loadings, measured by ICP-OES, were found in the range 0.2–0.36 wt% (Table 2) compared to the theoretical 0.25 wt%. Differences were attributed to experimental errors during synthesis and/or digestion of the samples.

STEM and EDS analyses were carried out to have an insight into the sizes of palladium species. It was difficult to discriminate between Pd and/or PdO particles and the supports' particles due to the small metal quantity and/or its high dispersion (Fig. 3A–D), precluding the measuring of an statistical average size of metal domains. However, we could infer a heterogeneous metal distribution since some Pd particles in the range of 4–5 nm but also around 20 nm were found in Pd/Ti5 catalyst. Moreover, we could scarcely observe metal particles in the range of 4–6 and 5–10 nm for Pd/Ti45 and Pd/Ti120 respectively [48]. These observations sustained previous XRD results, where PdO reflection could only be seen in Pd/Ti5, and thus bigger metal particles could be expected in this catalyst. Furthermore, it has been found that several solids submitted to mechanochemical activation exhibited an improved sorption capacity of divalent heavy metals from solution [49,50]. This behavior could also be extrapolated to the case of Pd^{2+} cations (from $PdCl_2$ precursor) present in the impregnation solutions used in this study to add Pd on titania supports. The quantity of defects obtained in the supports by milling process, and their distribution, could therefore act as active centers for the adsorption of metal particles and increase the dispersion of metallic domains on the surface [28,49,50]. Along with this behavior, smaller average metal domains could also be expected when using low metal amounts, as reported by other authors [51]. Particularly, the heterogenous distribution of metal particles found in Pd/Ti5 could be attributed to the slight mechanochemical activation of the support and the major presence of anatase crystal phase. Moreover, Debecker et al. [28] have demonstrated that a support composed of a mixture of TiO_2 crystal structures (anatase and rutile) dictates the morphology and dispersion of Ru species owing to lattice matching and enhanced stability (impeding sintering) upon annealing. Hence, different metal-support interactions could be achieved according to the crystalline phases present in the catalysts, changing both dispersion and oxidation state of palladium particles [28]. Subsequently, an XPS study was performed to elucidate surface chemistry of each catalyst.

Table 2
XPS and ICP-OES analyses of catalysts.

Catalyst	at%, theoretical	at%, XPS	wt%, theoretical	wt%, ICP-OES
	Pd/Ti	Pd/Ti	Pd	Pd
Pd/Ti5	0.19	0.39	0.25	0.20
Pd/Ti45		0.51		0.29
Pd/Ti120		0.64		0.36

3.4. XPS analyses

At the Ti 2p level, Pd/Ti5 presented Ti $2p_{3/2}$ and Ti $2p_{1/2}$ doublets (Fig. 4 A and Table 3) with binding energies (BE) values close to the ones reported for Ti^{4+} in anatase (458.59 eV and 464.31 eV respectively) [52]. These signals were shifted to higher BE compared to the supports (458.37 and 464.04 eV respectively), indicating certain degree of metal-support interaction after palladium addition [27]. Ti $2p_{1/2}$ could also be deconvoluted into a low-intensity signal attributed to Ti^{3+}. In case of Pd/Ti45 and Pd/Ti120, doublets presented BE with values close to the ones reported for Ti^{4+} in rutile (458.46 eV and 464.23 eV respectively) [52]. For both cases these signals could be mainly assigned to Ti^{4+} from TiO_2 (II) phase since the two catalysts contained between 40 and 50% of this crystalline phase. Moreover, signals shifted to lower BE after palladium addition when compared to the supports. This could be attributed to a partial reduction of Ti^{4+} to Ti^{3+} generating oxygen vacancies, as reported by other authors [15]. In line with this observation, both catalysts also presented a low-intensity signal located around 460.3 eV and assigned to Ti^{3+} at Ti $2p_{1/2}$ level.

At the Pd 3 d level, obtained signals were deconvoluted into four peaks (Fig. 4 B and Table 3) corresponding to Pd^0 (reference values of 334.7 eV for Pd $3d_{5/2}$ and 340.4 for Pd $3d_{3/2}$) and PdO (reference values of 336.2 eV for Pd $3d_{5/2}$ and 341.4 for Pd $3d_{3/2}$). We selected Pd $3d_{5/2}$ signals for interpretation of palladium oxidation state (Table 3). In case of Pd/Ti5, signals shifted to lower BE than the values reported for Pd^0 and PdO, indicating metal-support interaction even in non-reduced catalysts. For Pd/Ti45 and Pd/Ti120, these signals shifted to the opposite direction (higher BE) also indicating a metal-support interaction, but different from Pd/Ti5. Shifts to higher BE for Pd^0 have been usually associated to smaller particles of Pd [22]. This is in line with our STEM observations, were Pd/Ti45 and Pd/Ti120 showed smaller metallic domains than Pd/Ti5.

For Pd/Ti5, the shifts to higher BE for Ti 2p and lower BE for Pd 3 d could indicate an electronic transfer from support to metal, as observed by Namdeo et al. [3] for Pd/TiO_2 catalysts. This behavior was attributed to a possible formation of $TiPd_xO$ structures where palladium oxidation state could be more negative than zero [3,37]. Due to the high electronegativity of Ti, a charge transfer from support to metal could be expected, generating an electron cloud towards palladium [3]. In line with this explanation, Pd/Ti5 catalyst presented the highest content of Pd^0 (34.7%). According to Murata et al. [53], Pd^0–PdO interfaces are more active in C–H dissociation of methane than PdO or metallic Pd. In our case, the presence of Pd^0/PdO interfaces in the catalysts could be beneficial for glycerol oxidation in liquid phase in terms of OH^- adsorption and glycerol dehydration to glyceraldehyde intermediate [8,12].

The opposite shifts observed for Pd/Ti45 and Pd/Ti120 to lower BE in Ti 2p and higher BE in Pd 3 d could be associated to an electronic transfer from small metal particles to support, generating oxidized species ($Pd^{\delta+}$ with $\delta \geq 2$) and/or Pd/PdO_x interfaces [3,54]. Dodson et al. [15] reported a higher content of these species in rutile phase. In our case, both catalysts share a great quantity of TiO_2 (II) phase (43.3 and 49.4 wt% respectively) and an upward trend in rutile (8.3 and 27.6 wt% respectively) which might be the cause of the opposite electron transfer compared to the almost pure anatase present in Pd/Ti5. These results shed a light on the importance of grain boundaries in polymorphic transformations, which could change the direction of electron density transfer between metal and support, affecting speciation and catalytic properties of materials. Increased number of defects, and content of rutile and TiO_2 (II) phases in the supports milled for longer

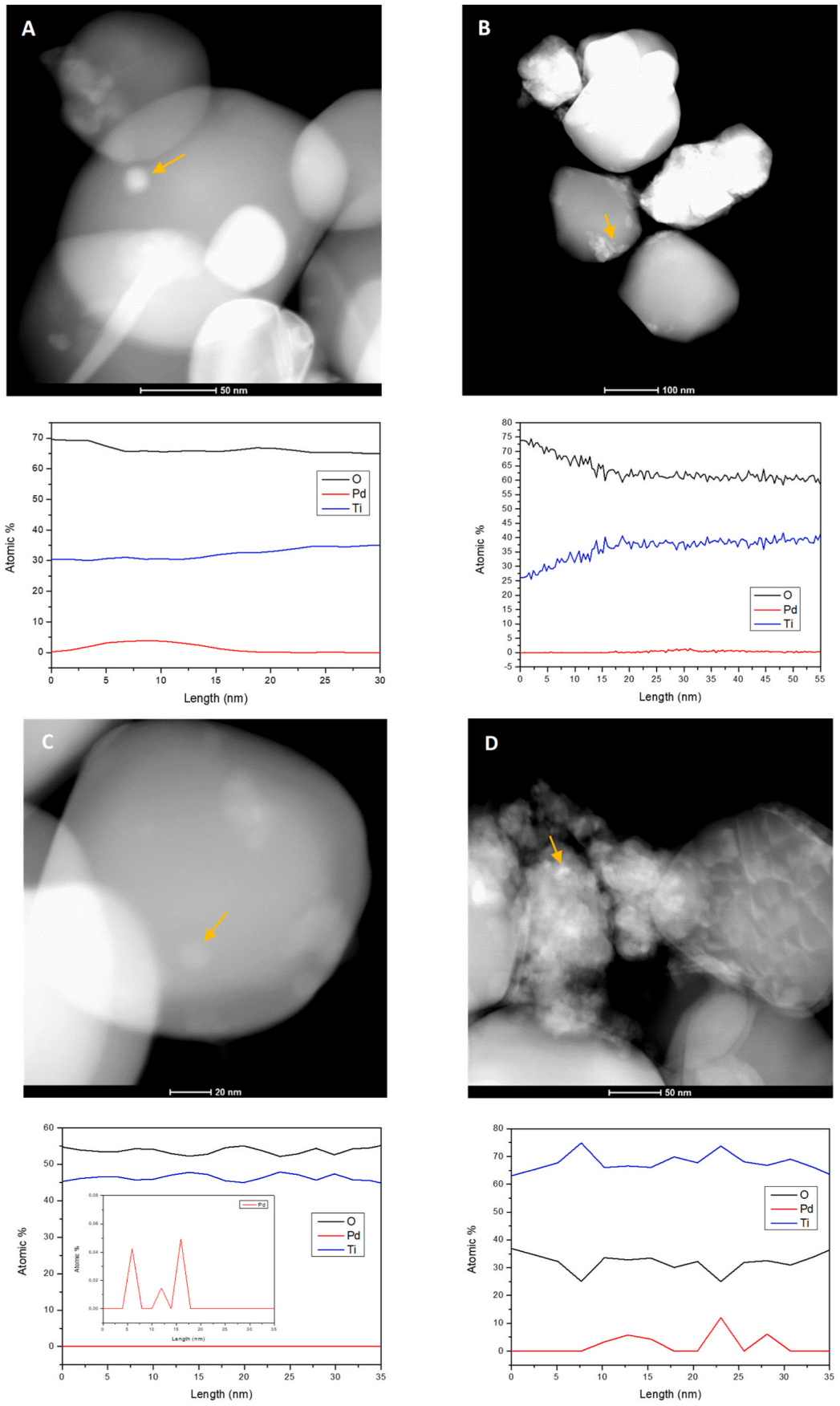

Fig. 3. STEM images and EDS analyses: Pd/Ti5 (A* and B), Pd/Ti45 (C) and Pd/Ti120 (D). *Reproduced with permission from ref. [43].

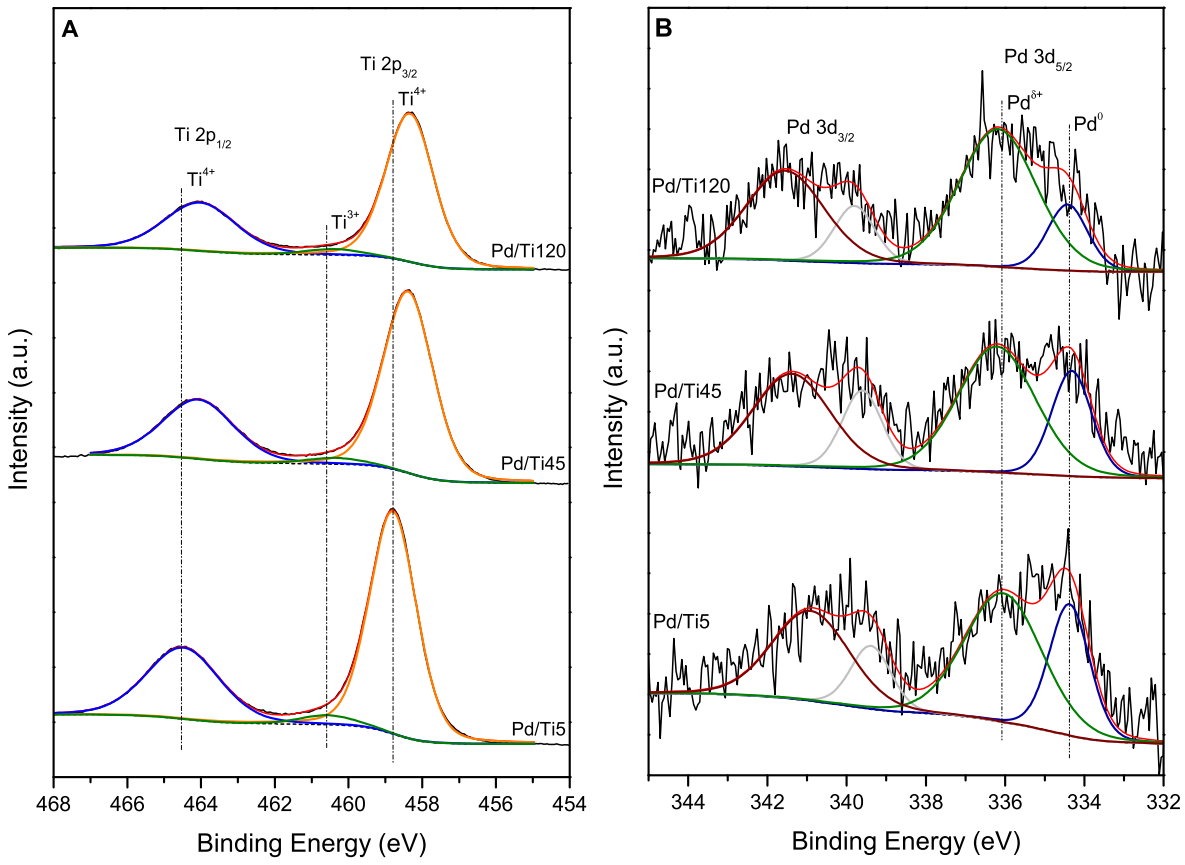

Fig. 4. XPS spectra of Ti 2p (A) and Pd 3 d (B) of catalysts.

Table 3
XPS analyses of catalysts.

Catalyst	Binding Energy (eV)							at%, XPS		at. ratio, XPS
	Ti $2p_{3/2}$ (Ti^{4+})	Ti $2p_{1/2}$ (Ti^{4+})	Ti $2p_{1/2}$ (Ti^{3+})	O 1s (O_{lat})	O 1s (O_{ads})	Pd $3d_{5/2}$ (Pd^0)	Pd $3d_{5/2}$ ($Pd^{\delta+}$)	$Pd^0/(Pd^0 + Pd^{\delta+})$	$O_{ads}/(O_{lat} + O_{ads})$	Ti/O_{lat}
Pd/Ti5	458.79	464.48	460.56	529.73	531.06	334.37	336.04	34.70	16.26	0.45
Pd/Ti45	458.38	464.06	460.33	529.65	531.22	334.32	336.21	30.33	10.10	0.42
Pd/Ti120	458.33	464.02	460.40	529.58	531.07	334.42	336.18	20.04	10.42	0.42

time would lead to more electron-deficient palladium species (oxidation states higher than zero) due to electron migration from palladium to titanium, as can be seen in $Pd^0/(Pd^0 + Pd^{\delta+})$ trend (Table 3) [14,15,17]. Cationic species of palladium and/or Pd/PdO boundaries obtained in the three catalysts are expected to accelerate the mechanism of glycerol oxidation [3,8]. Additionally, from the point of view of transfer-induced electrostatic interactions, the sintering of positively charged palladium particles demands more energy than zero valence palladium particles [17]. Therefore, the availability of cationic species on the surface may also stabilize the catalysts under reaction cycles, preventing a high rate of sintering.

Pd/Ti at% (Table 2) were in all cases higher than the theoretical calculation for the bulk (0.19 at%) but similar when affected by S_{BET}, which sustained the dispersion of Pd on the surface of supports [16].

O 1s level was deconvoluted into two signals (Fig. 5 and Table 3) associated to lattice oxygen (O_{lat}) (ca. 529.9 and 529.7 eV for anatase and rutile respectively) and oxygen adsorbed on oxygen vacancies (O_{ads}) (ca. 531.09 and 531.22 eV for anatase and rutile respectively) [52]. In case of Pd/Ti5, O_{lat} showed a BE close to the value reported for anatase while in Pd/Ti45 and Pd/Ti120 this value was closer to the BE for rutile, in accordance with the crystalline phases coexisting in the catalysts. Also, Ti/O_{lat} atomic ratios (Table 3) were in all cases lower that the theoretical (0.5) which may give evidence of certain number of oxygen vacancies present in the catalysts. In line with these values, Pd/Ti5 showed the higher O_{ads} quantity, 16.26%, while Pd/Ti45 and Pd/Ti120 showed values in the order of 10%. These contents were in the same order as observed in the supports [27], with a slight variation ascribed to palladium addition and further calcination. These low values of O_{ads} achieved after milling were previously explained in terms of oxygen vacancies migration from the surface to the bulk in order to induce polymorphic transformation during the synthesis of supports [27]. Distinctive properties observed in the three catalysts might have a decisive role on activity and selectivity during glycerol oxidation, where charge and oxygen mobility are key factors.

In order to emphasize support's milling effect, we decided to prepare and analyze a catalyst composed of 0.25 wt% palladium using pristine TiO_2 support (anatase, S_{BET} of 8 $m^2\ g^{-1}$) [27] and labeled it Pd/Ti. At the Ti 2p level we obtained signals in the order of reported ones for anatase phase with no substantial shifts in binding energies. In case of O 1s we observed an O_{ads} quantity of 23%, displaying some degree of surface

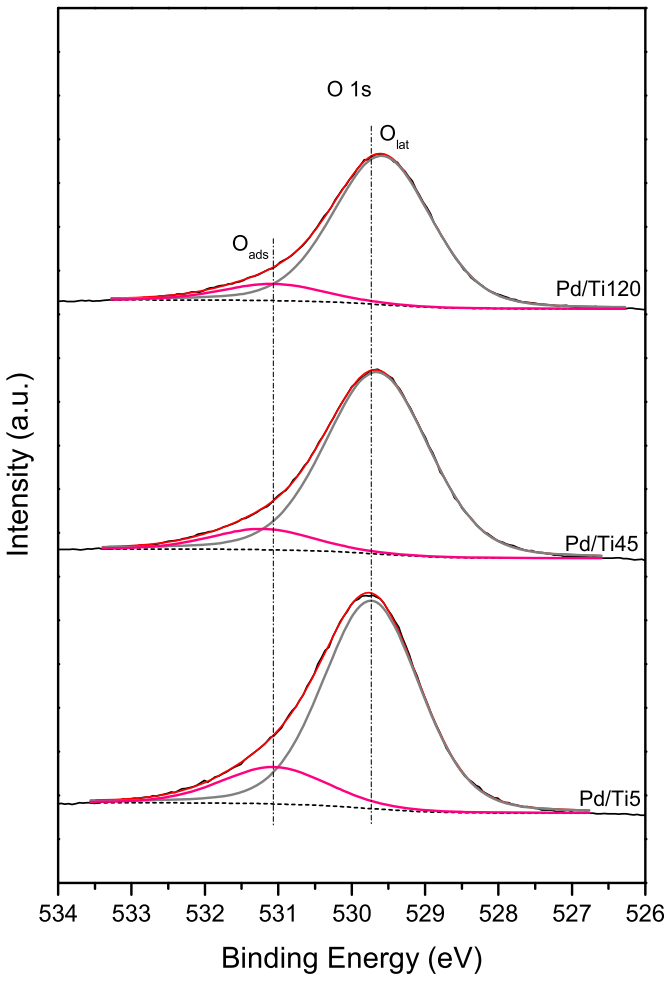

Fig. 5. XPS spectra of O 1s of catalysts.

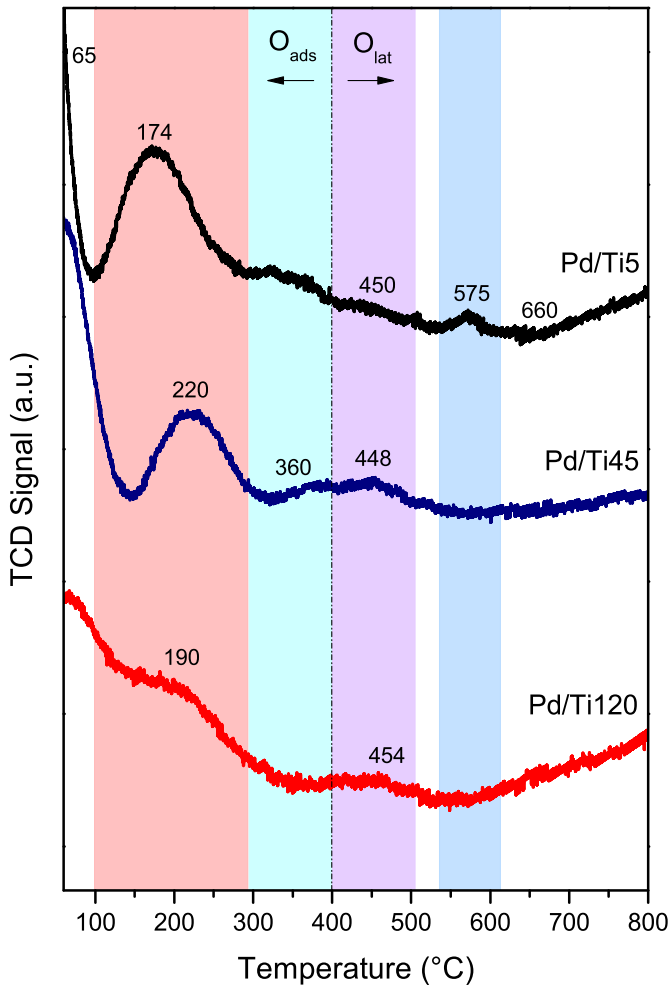

Fig. 6. O_2-TPD of catalysts.

oxygen vacancies, in agreement with its support [27]. More interestingly, deconvoluted Pd $3d_{5/2}$ signals gave values of 338.23 and 339.46 eV, indicating the only presence of cationic palladium species [55]. Since no substantial shifts in Ti 2p signals were observed, we could deduce a negligible metal-support interaction in this catalyst, where $Pd^{\delta+}$ species would be a consequence of surface oxygen in pristine titania. These results allowed us to remark that even a short milling time could provoke the support's 'activation' and benefit metal-support interaction, inducing electron migration according to the defects introduced and the TiO_2 polymorphs achieved.

To deepen in the study of oxygen mobility and oxygen species present in the catalysts, of vital importance in oxidation, we carried out O_2-Temperature Programmed Desorption (O_2-TPD) experiments.

3.5. O_2-TPD analyses

Ouyang et al. [56] reported different oxygen species for O_{ads} signals including oxygen from the surface of palladium particles and oxygen from the surface and subsurface of supports. Desorption signals (Fig. 6) found below 100 °C were related to oxygen species weakly bonded to the surface, as reported by other authors [57,58]. On the other hand, desorption signals located around 450 °C have been associated to surface lattice oxygen from the support [27]. These signals were observed at higher temperatures when compared to the supports, which could be explained by the metal-support interaction experienced after palladium addition, making oxygen release more difficult. Signals in the range 174–220 °C were attributed to oxygen species adsorbed on oxygen vacancies [59]. These oxygen species at the surface could be involved in the formation of oxygenated palladium species, with stronger bonds, that therefore desorb at higher temperatures. This fact could explain the disappearance of several low-temperature signals that were observed in the supports [27]. Also, the higher intensity and lower temperature of the desorption peak at 174 °C observed in Pd/Ti5 could be associated to the greater quantity of oxygen vacancies exhibited by XPS (Table 3). Furthermore, according to Ouyang et al. [56] signals located close to 200 °C could be attributed to molecular oxygen adsorbed on palladium particles, since they observed them in Pd black reference. Signals near 350 °C could be associated to the desorption of oxygen from finely dispersed PdO while the signal at 575 °C, only observed in Pd/Ti5, might be related to oxygen from larger PdO particles, as reported by Huang et al. [58]. These observations also have a good correlation with the palladium particles inferred by STEM, with larger sizes for Pd/Ti5 and smaller sizes for Pd/Ti45 and Pd/Ti120, leading to more oxygen-active species in the former. Catalysts with higher oxygen mobility are then expected to promote glycerol selective oxidation, in terms of oxygen supply and/or regeneration of the active surface [12,30,60].

3.6. H_2-TPR analyses

Grain boundaries and interfaces between titania phases and/or palladium could increase charge mobility and thus reducibility of the catalysts [32]. H_2-TPR measurements were performed to further study metal-support interactions, that play a major role in catalytic reactions that proceed via redox cycle [53]. Strong signals found in the range 533–578 °C (Fig. 7) were associated to the reduction of surface Ti^{4+}

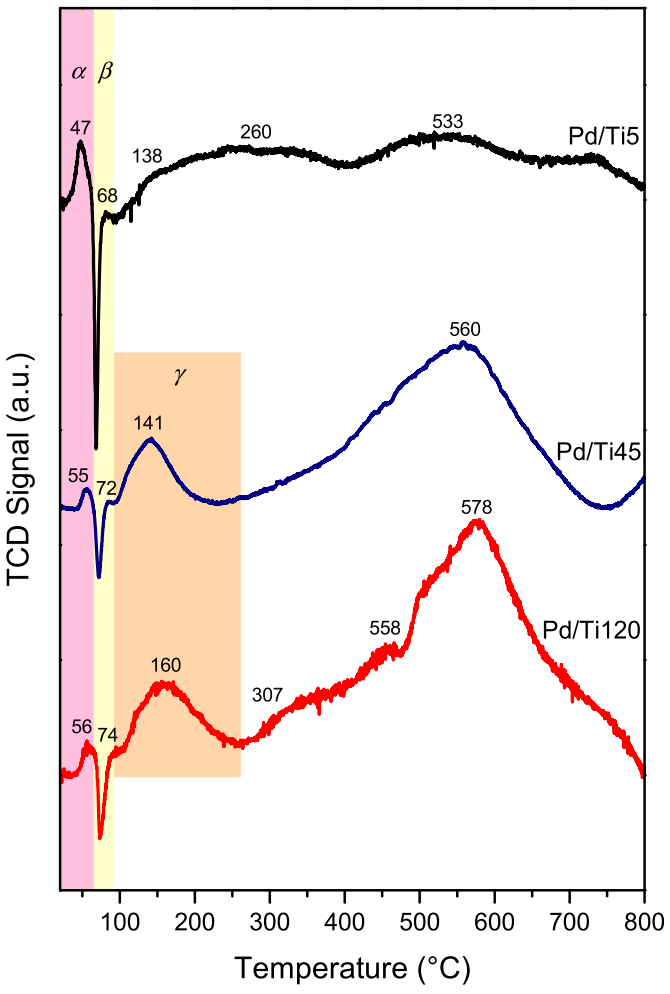

Fig. 7. H_2-TPR of catalysts.

[27]. These signals were obtained at lower temperatures compared to the supports, which could be attributed to an increase in reducibility due to palladium addition, as reported by other authors [61,62]. The broader and more intense signals observed in Pd/Ti45 and Pd/Ti120 catalysts were related to the longer milling time of its supports, which generates structures with improved oxygen diffusion and reducibility [14,27]. Likewise, the presence of Pd^0 particles could also induce the reduction of surface TiO_2, which may be associated to the low-intensity signals observed in the range 250–310 °C [61].

Positive signals found at low temperatures (α zone) were ascribed to the reduction of PdO to Pd^0 and the formation of β-PdH_x, after H_2 chemisorption on metallic palladium, that takes place even under reduction at ambient temperature [3,14,63,64]. H_2 uptakes showed values of 1.09, 0.25 and 0.47 μmol H_2 g^{-1} for Pd/Ti5, Pd/Ti45 and Pd/Ti120 respectively, which follow the trend of palladium particles sizes observed by STEM. Negative signals (β zone) were attributed to the decomposition of formed hydrides, releasing the H_2 [14,62,64]. Furthermore, these signals were related to the contribution of Pd^0 formed in α zone and the metallic palladium from fresh catalysts, to form the hydrides. Moreover, these signals have been associated to catalysts with larger Pd particles (>2 nm) since its easier for H_2 to form hydrides over larger metallic areas [61,64]. Bratan et al. [46] suggested that the tendency to form hydrides increases with palladium dispersion. Therefore, the presence of hydrides in the three catalysts could be the result of a good palladium dispersion despite the low concentration (0.25 wt%). Additionally, hydrides from small Pd particles decompose at higher temperatures than in large particles, as evidenced by other authors [64].

This observation is in line with our XRD and STEM results since Pd/Ti5 presented larger particles (~20 nm) and a more intense negative signal located at lower temperature, with an H_2 release of 1.26 μmol g^{-1}, compared to Pd/Ti45 and Pd/Ti120 catalysts (particle sizes in the order 4–6 nm and 5–10 nm respectively) with signals at higher temperatures and H_2 releases of 0.37 μmol g^{-1} and 0.27 μmol g^{-1} respectively. According to these results, XPS and O_2-TPD, a strong metal-support interaction in Pd/Ti5 could explain the characteristic reducibility, oxygen and hydrogen mobility in this catalyst.

Likewise, signals in the range 138–160 °C (γ zone) were associated to the reduction of PdO strongly interacting with titania support [62]. In case of Pd/Ti45 and Pd/Ti120, well-defined signals with maximums at 141 and 160 °C (respectively) were attributed to an enhanced reduction of PdO_x species. This increase in reducibility was related to the greater number of defects, lattice oxygen mobility and quantity of PdO_x species present in these catalysts, in line with previous results [14,27]. Enhanced redox properties and metal-support interaction observed could improve activity and selectivity of catalysts, but also increase the stability of active species under reaction conditions, avoiding metal sintering and leaching [60].

3.7. 2-Propanol decomposition test

2-propanol (isopropanol) decomposition has been extensively used as reaction test to study acid-base properties of active sites present in catalysts [65,66]. In general, it has been stated that 2-propanol dehydrates to propylene and/or isopropyl ether over acid centers and dehydrogenates to acetone over basic sites but also on acid-base pair sites or redox centers [65,67]. Moreover, conversion is attributed to the total number of active sites, acid or basic, while selectivity corresponds to specific sites for dehydration or dehydrogenation [65]. Conversion and selectivity of supports and catalysts were normalized per sample mass and S_{BET} (Table 4). Propene and acetone were the only products detected, with no evidence of isopropyl ether, carbon dioxide, water, or other possible reaction products. In case of supports, we observed an increase in conversion according to the extent of milling time. Selectivity to propene followed the same trend and neither acetone nor other products of reaction were detected. The absence of acetone could be a consequence of a small number of basic sites on the surface of supports. Furthermore, titania is considered to have a weakly acid surface, particularly associated to the presence of Lewis acid sites (Ti^+) and at a minor extent to Brønsted acid sites (Ti–OH) on the surface [68,69]. The increase in conversion and selectivity to propene could then be related to the grain disordered regions introduced by milling, which could act as active centers for 2-propanol decomposition [70,71]. Hence, acid-base properties of solids are sensible to bulk and surface modifications, including phase transformations and changes in microenvironments [23]. In case of catalysts, an evident drop in conversion was observed and associated to the addition of Pd and calcination at 500 °C, which could cause a loss and/or blockage of acid active sites generated by milling [70,72,73]. On the other hand, selectivity to propene was also lower but followed the same trend as in the supports, confirming the presence of Lewis and/or Brønsted sites on catalysts' surface. A lower

Table 4
Conversion and product selectivity of supports and catalysts for 2-propanol decomposition.

Sample	Conversion (%)	Selectivity (%)	
		Propene	Acetone
Ti5	5	11	0
Ti45	15	77	0
Ti120	25	86	0
Pd/Ti5	3	3	5
Pd/Ti45	9	10	6
Pd/Ti120	6	29	5

but similar selectivity to acetone was also observed and attributed to palladium addition, which could increase basic and/or acid-base pair sites, but also contribute with metallic sites for alcohol dehydrogenation, as reported by other authors [72,74]. In order to dig deeper into surface basicity of catalysts we calculated the ratio between selectivity to acetone and selectivity to propene, obtaining the trend: Pd/Ti5 > Pd/Ti45 > Pd/Ti120 with values of 1.54, 0.60 and 0.18 respectively. This tendency could be associated to the presence of palladium in contact with an almost pure anatase phase in former catalyst and the progressive loss of this phase in the latter catalysts, replaced by defective structures of TiO_2 (II) and rutile, that are known to show low basicity [13,75]. Moreover, distinctive metal-support interaction discussed previously for Pd/Ti5 and its greater O_{ads} quantity could also be the cause of a higher basicity and/or a greater number of surface acid-base pairs related to redox properties. The presence of this kind of active sites on the surface of catalyst would promote first step of deprotonation during alcohol oxidation reactions [8,12,73].

An unique metal oxide support (titania in this case) with different polymorphic mixtures obtained by high-energy ball milling could therefore generate catalysts with different acid-base properties. The distinctive active centers obtained, and the reaction conditions used, could also alter the way reactants interact with the catalytic surface, changing conversion and/or selectivity during a particular reaction. It has been reported that, under base-free conditions, supports with Lewis and Brønsted acid sites would favor selectivity to lactic acid, while catalysts mainly composed of basic sites (particularly associated to deposited metal, presence of NaOH and oxygen) would direct glycerol oxidation to produce glyceric acid [76,77]. Considering surface acid/-base features achieved in present catalysts and reaction conditions employed, both products could be obtained, as further explained in the following section.

3.8. Catalytic activity

Catalysts and supports were tested as obtained without previous reduction to simplify synthesis process, thinking in a scale-up possibility, and to preserve cationic species of palladium that could benefit hydroxyl adsorption and further proton subtraction from glycerol molecule [8,12].

Conversion and selectivity to products (Fig. 8 A and B) were obtained for all samples under the same conditions previously mentioned. Homogeneous reaction with NaOH and absence of catalyst showed the importance of a base for oxidation initiation, obtaining a conversion of 37% and lactic (LA) and formic acids (FA) as major products. Supports displayed significant catalytic activity by themselves, which could be attributed to the strong electron-withdrawing ability of Ti surface atoms, activating primary hydroxyl group of glycerol [21]. A slight decrease in conversion (Ti5>Ti45 > Ti120) was observed, in line with anatase content of each support. Moreover, surface acidity and conversion were inversely proportional, obtaining the highest conversion and selectivity to glyceric acid (GA), LA and FA for Ti5. This behavior could also be attributed to the greater number of oxygen vacancies and low acidity of aforementioned support [10,27]. Carbon balance gives us information about conversion efficiency during oxidation reaction. Values observed in all cases demonstrate that other intermediate products such as tartronic, glycolic and glyoxylic acids could also be obtained. Moreover, C–C cleavage leading to CO_2 as complete oxidation product is expected as well [3,13].

In case of catalysts, higher conversion and selectivity to acid products were observed, elucidating the role of palladium particles. Conversion followed the trend Pd/Ti5»Pd/Ti45 > Pd/Ti120, also in line with anatase content and acetone:propene selectivity ratio observed in our previous 2-propanol decomposition test, with the highest glycerol conversion of 94% obtained for Pd/Ti5 and selectivity to GA and LA of 48% and 22% respectively. Small quantities of oxalic acid (OA) and FA were also observed, as expected for the reaction network of glycerol

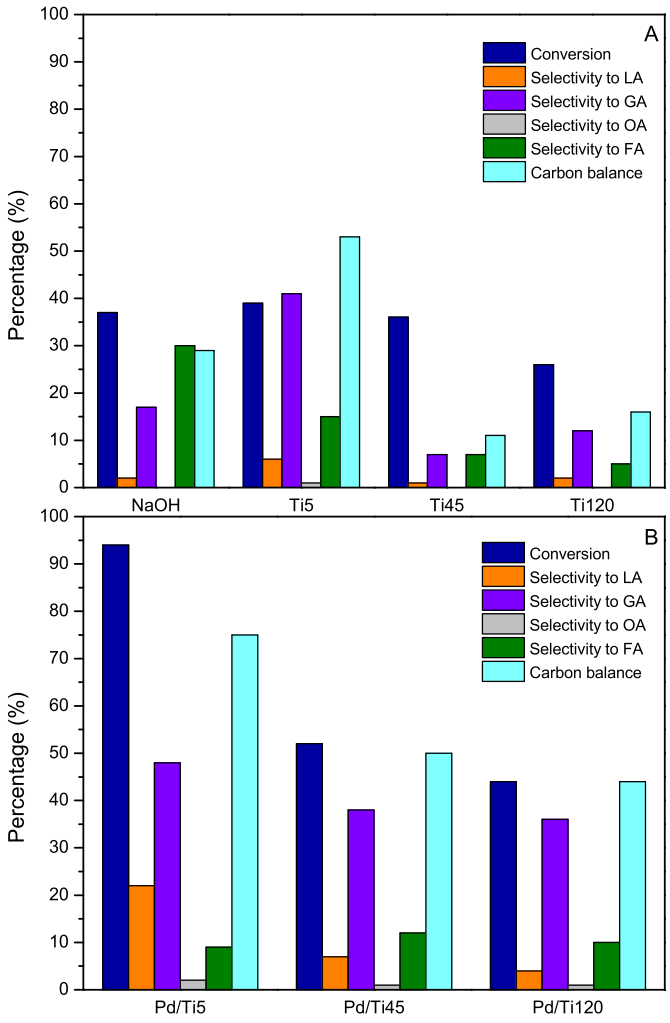

Fig. 8. Glycerol conversion and product selectivity for supports (A) and catalysts (B). Reaction conditions: 0.15 mol/L GLY, 1 bar O_2, NaOH:GLY = 2, Pd:GLY = 600, 100 °C, 1000 rpm, 4 h.

oxidation [8]. Zhang et al. [78] attributed the increase in GA selectivity to C–C cleavage inhibition due to longer Ti–Ti distance in anatase. Furthermore, glycerol selectivity enhancement could be attributed to the increase in basicity and/or decrease in acidity observed, as reported by other authors [10,79]. Greater Pd particles found in this catalyst might also be associated to the higher conversion and selectivity to glyceric acid, as reported in literature [79,80]. In line with these results, glycerol conversion, GA and LA selectivity followed the same trend as carbon balance, indicating the degree of partial oxidation efficiency in each catalyst. We also tested palladium supported on pristine TiO_2 to elucidate the contribution of pure anatase and defective anatase on glycerol oxidation. As expected, we obtained equal conversion but lower selectivity to GA, LA and FA of 43%, 11% and 9% respectively and a carbon balance of 61% (compared to 75% in Pd/Ti5). Superior catalytic performance of Pd/Ti5 could therefore be ascribed to the metal-support interaction and oxygen mobility along palladium, induced by defective grain boundaries of anatase achieved by mechanochemical activation for a short milling time [27,48,70].

On the other hand, Pd/Ti45 and Pd/Ti120 showed a downward trend in conversion and selectivity to GA and LA. Zhang et al. [78] reported catalysts of Pt nanoparticles supported on different TiO_2 crystal structures (anatase and rutile) to understand the effect of the support on glycerol selective oxidation. They found that, even though Pt/TiO_2 catalysts had a slight difference in conversion, exhibited great differences of selectivity to intermediate glyceraldehyde (GLYAD) and GA.

They could calculate apparent activation energies (Ea) of the critical reaction steps, using GLYAD and GA as reactants, where GLYAD oxidation was 18.15 kJ/mol on Pt/R (rutile) and 31.27 kJ/mol on Pt/A (anatase). In case of GA oxidation Ea values were also in the order Pt/R < Pt/A, which indicated that Pt/A catalyst was less effective in C–C cleavage. Additionally, they also performed FTIR and Raman analyses and found that intermediate GLYAD was highly dissociated in a bidentate form through C atom bonding to O atom and the O atom to Ti atom in Ti–O site of rutile, which promoted GLYAD transformation to GA. They could also demonstrate that formed GA would then be bridging absorbed through two O atoms bonding to the Ti atoms of $(Ti–O–Ti)_{(110)}$ sites with a proper Ti–Ti distance, which inevitably led to the generation of undesired C–C cleavage product over Pt/R catalyst. On the contrary, they found that GLYAD molecule dissociated in a monodentate form over Ti–O sites of anatase which was not beneficial to the transformation from GLYAD to GA. Fortunately, they found that the C–C cleavage of GA was weakened on the $(Ti–O–Ti)_{(101)}$ sites of anatase support due to the longer Ti–Ti distance, indicating that the role of (Ti–O–Ti) sites of the support could regulate the adsorption of an intermediate/product. These results were in line with the catalytic performance of our catalysts. Anatase (a = 3.7852 Å) is the major phase present in Pd/Ti5 and showed the highest selectivity to GA and the best carbon balance. Though, in case of Pd/Ti45 and Pd/Ti120 catalysts, both values declined with the increase in rutile (a = 4.5933 Å) and TiO_2 (II) (a = 4.5150 Å) present in the supports, with similar cell parameters compared to anatase.

As well, the more acid surfaces present in these catalysts seemed to provoke a different adsorption/desorption performance of reactants and products. The slight increase in FA selectivity and the decrease in carbon balance, due to overoxidation and CO_2 formation, could also be attributed to the greater oxygen activation observed by H_2-TPR and O_2-TPD for Pd/Ti45 and Pd/Ti120 [21,78].

Pd/Ti5 was selected to examine its stability under recycling tests (Fig. 9). After oxidation reaction completion, catalyst was recovered, washed with milliQ water and dried in an oven at 70 °C under air to be tested in a new reaction at the same operational conditions. Deactivation observed after catalytic cycles could be associated to reactant and/or product adsorption on the surface and inside de pores, decreasing the availability of active sites [21,81]. Particularly, glyceric and tartronic acids tend to adsorb irreversibly on catalysts' surface, inhibiting activity, due to their chelating properties [13]. This behavior could lead to the observed decrease in GA and LA selectivity and the increase in FA selectivity, due to overoxidation of glycerol and/or product molecules to lower carbon products [13,21]. Moreover, carbon balance values also showed a probable total oxidation to CO_2. To sustain this hypothesis, we recovered Pd/Ti5 catalyst after the third catalytic test and submitted it to Thermogravimetric Analysis (TGA) and XPS. From TGA (up to 700 °C), we obtained a weight loss of 0.87% with two events at 350 and 550 °C that could be associated to organic molecules decomposition [82,83]. Furthermore, Pd/Ti atomic ratio from XPS remained unchanged, indicating no lixiviation of palladium species. $Pd^0/(Pd^0 + Pd^{\delta+})$ ratio decreased from 34.70 to 13.89 after three consecutive oxidation reactions, increasing cationic species of palladium, which could also explain the observed decline in catalytic activity. C 1s could be deconvoluted into 4 signals (instead of 2 in fresh catalysts) where, according to the literature [84], the new ones were attributed to carbonyl groups (288.8 and 291.8 eV), showing the presence of some new carbon molecules at the surface. In addition, O 1s deconvolution presented a third signal at 533.7 eV commonly associated to OH groups and water, in line with the feasible adsorption of glycerol and/or carboxylic acids on the surface [13,55].

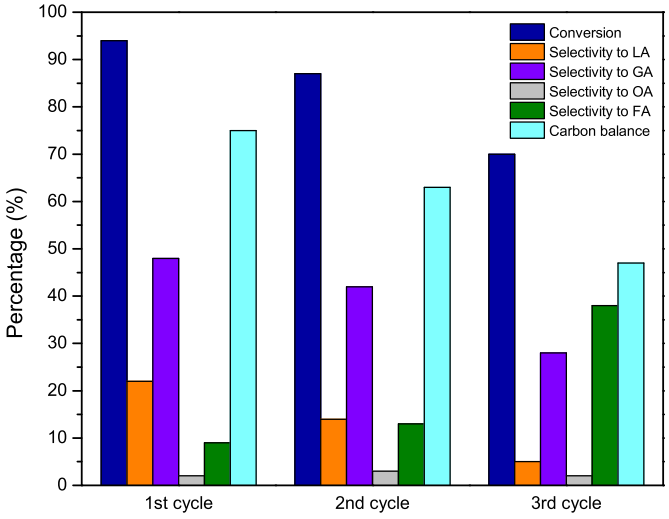

Fig. 9. Pd/Ti5 stability under recycling tests. Reaction conditions: 0.15 mol/L GLY, 1 bar O_2, NaOH:GLY = 2, Pd:GLY = 600, 100 °C, 1000 rpm, 4 h.

4. Conclusions

Since supports not only serve as carriers for active metals but also could affect overall performance of supported catalysts, they need to be considered when designing a particular catalyst. In this way, support's modification by high-energy ball milling emerges as an advantageous way to obtain diverse physicochemical properties for defined applications. Herein, defective mixes of anatase, TiO_2 (II) and rutile crystalline phases, obtained in a previous work, were used as supports for palladium catalysts and further tested on glycerol selective oxidation. Defects and boundaries between polymorphic phases of titania could not only affect acid-base character but also modify the direction of electron transfer between metal and support, changing redox properties and oxygen mobility of final catalysts. Pd/Ti5 catalyst displayed a charge transfer from Ti to Pd in agreement with anatase phase of the support while the presence of more stable rutile in Pd/Ti45 and Pd/Ti120 catalysts, with lower surface energy, provoked an opposite charge transfer from Pd to Ti. Furthermore, reactants and products would adsorb/desorb in different ways over Pd/PdO sites, and/or Pd/PdO/support sites, due to distinctive metal-support interactions. Pd/Ti5, mostly composed of defective anatase, showed the best catalytic performance owing to greater Pd particles, higher basicity and/or redox features and C–C cleavage inhibition compared to Pd/Ti45 and Pd/Ti120, composed of different amounts of anatase, TiO_2 (II) and rutile. Present study highlights how a simple activation of commercial supports through a simple and eco-friendly technique, such us high-energy ball milling, allows the design of catalysts with specific functionalities, surface physical-chemistry and metal-support interactions, leading to different catalytic performances for a given reaction.

Credit author statement

Matías Gastón Rinaudo: Conceptualization, Investigation, Visualization, Writing – original draft, Review and Editing. **Ana María Beltrán**: TEM Measurements and Analyses, Validation, Writing – Review. **Asunción Fernández**: TEM Measurements and Analyses, Validation, Writing – Review. **Luis Eduardo Cadús**: Conceptualization, Validation, Supervision, Writing – Review. **Maria Roxana Morales**: Conceptualization, Validation, Resources, Supervision, Writing – Review.

Declaration of competing interest

The authors declare that they have no known competing financial interests or personal relationships that could have appeared to influence the work reported in this paper.

Data availability

No data was used for the research described in the article.

Acknowledgements

The authors acknowledge the Universidad Nacional de San Luis (UNSL), Agencia Nacional de Promoción Científica y Tecnológica (ANPCyT) and Consejo Nacional de Investigaciones Científicas y Técnicas (CONICET) for their financial support. Also, thanks are given to ANPCyT for the purchase of the SPECS multitechnique analysis instrument (PME8-2003) where XPS analyses were made. The authors also acknowledge the Spanish Ministry of Science and Innovation and Universities under grant no. RTI2018-093871-B-I00 and the Junta de Andalucía under grant no. P20_00239, both co-financed by EU FEDER funds. The University of Seville is also acknowledged for the use of its general research service (CITIUS).

References

[1] G. Dodekatos, L. Abis, S.J. Freakley, H. Tüysüz, G.J. Hutchings, Glycerol oxidation using MgO- and Al2O3-supported gold and gold–palladium nanoparticles prepared in the absence of polymer stabilizers, ChemCatChem 10 (2018) 1351–1359, https://doi.org/10.1002/cctc.201800074.

[2] M.R.A. Arcanjo, I.J. da Silva, C.L. Cavalcante, J. Iglesias, G. Morales, M. Paniagua, J.A. Melero, R.S. Vieira, Glycerol valorization: conversion to lactic acid by heterogeneous catalysis and separation by ion exchange chromatography, Biofuels, Bioprod. Biorefining. (2019) 1–14, https://doi.org/10.1002/bbb.2055.

[3] A. Namdeo, S.M. Mahajani, A.K. Suresh, Palladium catalysed oxidation of glycerol - effect of catalyst support, J. Mol. Catal. Chem. 421 (2016) 45–56, https://doi.org/10.1016/j.molcata.2016.05.008.

[4] S. Vajíček, M. Štolcová, A. Kaszonyi, M. Mičušík, P. Alexy, P. Canton, G. Onyestyák, S. Harnos, F. Lónyi, J. Valyon, Gel-type ion exchange resin stabilized Pd-Bi nanoparticles for the glycerol oxidation in liquid phase, J. Ind. Eng. Chem. 39 (2016) 77–86, https://doi.org/10.1016/j.jiec.2016.05.010.

[5] P. Chagas, M.A. Thibau, S. Breder, P.P. Souza, G.S. Caldeira, M.F. Portilho, C. S. Castro, L.C.A. Oliveira, Metal-free bifunctional silica for conversion of waste glycerol from biodiesel: sustainable production of formic acid, Chem. Eng. J. 369 (2019) 1102–1108, https://doi.org/10.1016/j.cej.2019.03.068.

[6] F.M. Perez, M.N. Gatti, N.N. Nichio, F. Pompeo, Bio-additives from glycerol acetylation with acetic acid: chemical equilibrium model, Res. Eng. 15 (2022), 100502, https://doi.org/10.1016/j.rineng.2022.100502.

[7] C. D'Agostino, G. Brett, G. Divitini, C. Ducati, G.J. Hutchings, M.D. Mantle, L. F. Gladden, Increased affinity of small gold particles for glycerol oxidation over Au/TiO2 probed by NMR relaxation methods, ACS Catal. 7 (2017) 4235–4241, https://doi.org/10.1021/acscatal.7b01255.

[8] M.S. Ide, R.J. Davis, The important role of hydroxyl on oxidation catalysis by gold nanoparticles, Acc. Chem. Res. 47 (2014) 825–833, https://doi.org/10.1021/ar4001907.

[9] M. Douthwaite, N. Powell, A. Taylor, G. Ford, J.M. López, B. Solsona, N. Yang, O. Sanahuja-Parejo, Q. He, D.J. Morgan, T. Garcia, S.H. Taylor, Glycerol selective oxidation to lactic acid over AuPt nanoparticles; enhancing reaction selectivity and understanding by support modification, ChemCatChem 12 (2020) 3097–3107, https://doi.org/10.1002/cctc.202000026.

[10] Y. Bin Choi, N. Nunotani, K. Morita, N. Imanaka, Selective glycerol oxidation to glyceric acid under mild conditions using Pt/CeO2–ZrO2–Fe2O3/SBA-16 catalysts, J. Asian Ceram. Soc. 10 (2022) 178–187, https://doi.org/10.1080/21870764.2022.2028980.

[11] S. Li, W. Deng, Y. Li, Q. Zhang, Y. Wang, Catalytic conversion of cellulose-based biomass and glycerol to lactic acid, J. Energy Chem. (2019) 138–151, https://doi.org/10.1016/j.jechem.2018.07.012.

[12] R.J.D. Bhushan N. Zope, David D. Hibbitts, Matthew Neurock, Reactivity of the gold/water interface during selective oxidation catalysis reactivity of the gold/water interface during selective oxidation catalysis, Science 330 (80-) (2010) 74–77, https://doi.org/10.1126/science.1191652.

[13] A. Namdeo, J.H. Jhaveri, S.M. Mahajani, A.K. Suresh, Palladium catalyzed liquid phase oxidation of glycerol under alkaline conditions - kinetic analysis and modelling, Chem. Eng. J. 438 (2022), 135424, https://doi.org/10.1016/j.cej.2022.135424.

[14] J. Zhu, W. Mu, L. Su, X. Li, Y. Guo, S. Zhang, Z. Li, Al-doped TiO2mesoporous material supported Pd with enhanced catalytic activity for complete oxidation of ethanol, J. Solid State Chem. 248 (2017) 142–149, https://doi.org/10.1016/j.jssc.2017.01.028.

[15] J.J. Dodson, H.E. Hagelin-Weaver, Effect of titania structure on palladium oxide catalysts in the oxidative coupling of 4-methylpyridine, J. Mol. Catal. Chem. 410 (2015) 271–279, https://doi.org/10.1016/j.molcata.2015.09.014.

[16] A. Kim, C. Sanchez, G. Patriarche, O. Ersen, S. Moldovan, A. Wisnet, C. Sassoye, D. P. Debecker, Selective CO2 methanation on Ru/TiO2 catalysts: unravelling the decisive role of the TiO2 support crystal structure, Catal. Sci. Technol. 6 (2016) 8117–8128, https://doi.org/10.1039/c6cy01677d.

[17] N. Wang, S. Li, Y. Zong, Q. Yao, Y. Zhang, Flame synthesis of novel ternary nanocatalysts Pd/CeO2-TiO2 with promotional low-temperature catalytic oxidation properties, Proc. Combust. Inst. 36 (2017) 1029–1036, https://doi.org/10.1016/j.proci.2016.08.060.

[18] T. Kandasamy, M. Banu, R. Vijaya Shanthi, S. Sivasanker, Suitability of different supported Ru, Pt and Ni catalysts for the hydrogenolysis of sorbitol, Res. Eng. 15 (2022), 100594, https://doi.org/10.1016/j.rineng.2022.100594.

[19] L.E. Oi, M.Y. Choo, H.V. Lee, H.C. Ong, S.B.A. Hamid, J.C. Juan, Recent advances of titanium dioxide (TiO2) for green organic synthesis, RSC Adv. 6 (2016) 108741–108754, https://doi.org/10.1039/c6ra22894a.

[20] W.J. Shen, M. Okumura, Y. Matsumura, M. Haruta, The influence of the support on the activity and selectivity of Pd in CO hydrogenation, Appl. Catal. Gen. 213 (2001) 225–232, https://doi.org/10.1016/S0926-860X(01)00465-3.

[21] G. Wu, Y. Liu, Y. He, J. Feng, D. Li, Reaction pathway investigation using in situ Fourier transform infrared technique over Pt/CuO and Pt/TiO2 for selective glycerol oxidation, Appl. Catal. B Environ. 291 (2021), 120061, https://doi.org/10.1016/j.apcatb.2021.120061.

[22] W. Cui, S. Li, D. Wang, Y. Deng, Y. Chen, High reactivity and sintering resistance of CH 4 oxidation over modified Pd/Al 2 O 3, Catal. Commun. (2019) 86–90, https://doi.org/10.1016/j.catcom.2018.10.028.

[23] G. Wang, W. Wang, F. Zhang, W. Gao, R. Cong, T. Yang, Octahedron-based gallium borates (Ga-PKU-1) with an open framework: acidity, catalytic dehydration and structure–activity relationship, Catal. Sci. Technol. 6 (2016) 5992–6001, https://doi.org/10.1039/c5cy02218e.

[24] B. Van Vaerenbergh, J. Lauwaert, P. Vermeir, J. De Clercq, J.W. Thybaut, Synthesis and Support Interaction Effects on the Palladium Nanoparticle Catalyst Characteristics, first ed., Elsevier Inc., 2019 https://doi.org/10.1016/bs.acat.2019.10.001.

[25] Z. Luo, D.A. Kriz, R. Miao, C.H. Kuo, W. Zhong, C. Guild, J. He, B. Willis, Y. Dang, S.L. Suib, P. Nandi, TiO2 Supported gold–palladium catalyst for effective syngas production from methane partial oxidation, Appl. Catal. Gen. 554 (2018) 54–63, https://doi.org/10.1016/j.apcata.2018.01.020.

[26] Z. Rui, S. Wu, C. Peng, H. Ji, Comparison of TiO 2 Degussa P25 with anatase and rutile crystalline phases for methane combustion, Chem. Eng. J. 243 (2014) 254–264, https://doi.org/10.1016/j.cej.2014.01.010.

[27] M.G. Rinaudo, A.M. Beltrán, M.A. Fernández, L.E. Cadús, M.R. Morales, Tailoring materials by high-energy ball milling: TiO2 mixtures for catalyst support application, Mater. Today Chem. 17 (2020), 100340, https://doi.org/10.1016/j.mtchem.2020.100340.

[28] A. Kim, D.P. Debecker, F. Devred, V. Dubois, C. Sanchez, C. Sassoye, CO2 methanation on Ru/TiO2 catalysts: on the effect of mixing anatase and rutile TiO2 supports, Appl. Catal. B Environ. 220 (2018) 615–625, https://doi.org/10.1016/j.apcatb.2017.08.058.

[29] S. Begin-Colin, T. Girot, A. Mocellin, G. Le Caër, Kinetics of formation of nanocrystalline TiO2 II by high energy ball-milling of anatase TiO2, Nanostruct. Mater. 12 (1999) 195–198, https://doi.org/10.1016/S0965-9773(99)00097-5.

[30] H. Zhu, Z. Qin, W. Shan, W. Shen, J. Wang, Pd/CeO2-TiO2 catalyst for CO oxidation at low temperature: a TPR study with H2 and CO as reducing agents, J. Catal. 225 (2004) 267–277, https://doi.org/10.1016/j.jcat.2004.04.006.

[31] S.B.A. Hamid, N. Basiron, W.A. Yehye, P. Sudarsanam, S.K. Bhargava, Nanoscale Pd-based catalysts for selective oxidation of glycerol with molecular oxygen: structure–activity correlations, Polyhedron 120 (2016) 124–133, https://doi.org/10.1016/j.poly.2016.07.017.

[32] S. Kityakarn, A. Worayingyong, A. Suramitr, M.F. Smith, Ce-doped nanoparticles of TiO 2 : rutile-to-brookite phase transition and evolution of Ce local-structure studied with XRD and XANES, Mater. Chem. Phys. 139 (2013) 543–549, https://doi.org/10.1016/j.matchemphys.2013.01.055.

[33] P. Dulian, M. Buras, W. Żukowski, Modyfication of photocatalytic properties of titanium dioxide by mechanochemical method, Polish, J. Chem. Technol. 18 (2016) 68–71, https://doi.org/10.1515/pjct-2016-0061.

[34] H. Dutta, Y.C. Lee, S.K. Pradhan, Microstructure characterization and polymorphic transformation kinetic study of ball-milled nanocrystalline a-TiO2-20 mol% m-ZrO2 mixture by X-ray diffraction and electron microscopy, Phys. E Low-Dimensional Syst. Nanostruct. 36 (2007) 17–27, https://doi.org/10.1016/j.physe.2006.07.042.

[35] O.C. Duvarci, M. Çiftçioğlu, Preparation and characterization of nanocrystalline titania powders by sonochemical synthesis, Powder Technol. 228 (2012) 231–240, https://doi.org/10.1016/j.powtec.2012.05.022.

[36] Z. Tan, P. Chen, Q. Zhou, J. Liu, X. Mei, B. Wang, N. Cui, Shock synthesis and characterization of titanium dioxide with α-PbO2 structure, J. Phys. Condens. Matter 30 (2018), https://doi.org/10.1088/1361-648X/aac709.

[37] D.S. García-Zaleta, A.M. Torres-Huerta, M.A. Domínguez-Crespo, A. García-Murillo, R. Silva-Rodrigo, R.L. González, Influence of phases content on Pt/TiO2, Pd/TiO2 catalysts for degradation of 4-chlorophenol at room temperature, J. Nanomater. 2016 (2016), https://doi.org/10.1155/2016/1805169.

[38] J. Miao, R. Zhang, L. Zhang, Photocatalytic degradations of three dyes with different chemical structures using ball-milled TiO2, Mater. Res. Bull. 97 (2018) 109–114, https://doi.org/10.1016/j.materresbull.2017.08.032.

[39] A. Gajovic Â, M. Stubic Ïar, M. Ivanda, K. Furic, Raman Spectroscopy of Ball-Milled TiO 2, 2001, https://doi.org/10.1016/S0022-2860(00)00790-0.

[40] X. Yao, R. Zhao, L. Chen, J. Du, C. Tao, F. Yang, L. Dong, Selective catalytic reduction of NOxby NH3over CeO2supported on TiO2: comparison of anatase, brookite, and rutile, Appl. Catal. B Environ. 208 (2017) 82–93, https://doi.org/10.1016/j.apcatb.2017.02.060.

[41] A. Gajović, K. Furić, N. Tomašić, S. Popović, Ž. Skoko, S. Musić, Mechanochemical preparation of nanocrystalline TiO2 powders and their behavior at high

temperatures, J. Alloys Compd. 398 (2005) 188–199, https://doi.org/10.1016/j.jallcom.2005.02.004.
[42] L. Martínez, M. Benito, I. Mata, L. Soler, E. Molins, J. Llorca, Preparation and photocatalytic activity of Au/TiO2 lyogels for hydrogen production, Sustain. Energy Fuels 2 (2018) 2284–2295, https://doi.org/10.1039/c8se00293b.
[43] C. Belver, M.J. López-Muñoz, J.M. Coronado, J. Soria, Palladium enhanced resistance to deactivation of titanium dioxide during the photocatalytic oxidation of toluene vapors, Appl. Catal. B Environ. 46 (2003) 497–509, https://doi.org/10.1016/S0926-3373(03)00291-1.
[44] S. Zaid, E. Skrzyńska, A. Addad, S. Nandi, L. Jalowiecki-Duhamel, J.S. Girardon, M. Capron, F. Dumeignil, Development of silver based catalysts promoted by noble metal M (M = Au, Pd or Pt) for glycerol oxidation in liquid phase, Top. Catal. 60 (2017) 1072–1081, https://doi.org/10.1007/s11244-017-0800-6.
[45] W. Hu, D. Knight, B. Lowry, A. Varma, Selective oxidation of glycerol to dihydroxyacetone over Pt-Bi/C catalyst: optimization of catalyst and reaction conditions, Ind. Eng. Chem. Res. 49 (2010) 10876–10882, https://doi.org/10.1021/ie1005096.
[46] R. Vujasin, A. Mraković, S. Kurko, N. Novaković, L. Matović, J.G. Novaković, S. Milošević, Catalytic activity of titania polymorphs towards desorption reaction of MgH2, Int. J. Hydrogen Energy 41 (2016) 4703–4711, https://doi.org/10.1016/j.ijhydene.2016.01.095.
[47] M. Ali, Ceramic processing research transformation and powder characteristics of TiO 2 during high energy milling, J. Ceramic Process. Res. 15 (5) (2014) 290–293.
[48] M.G. Rinaudo, A.M. Beltrán, M.A. Fernández, L.E. Cadús, M.R. Morales, Synthesis and characterization of Pd over novel TiO2 mixtures: insights on metal-support interactions, Chem. Process 2 (2020), https://doi.org/10.3390/eccs2020-07529.
[49] I. Tole, K. Habermehl-Cwirzen, A. Cwirzen, Mechanochemical activation of natural clay minerals: an alternative to produce sustainable cementitious binders – review, Mineral. Petrol. 113 (2019) 449–462, https://doi.org/10.1007/s00710-019-00666-y.
[50] P. Baláž, M. Achimovicová, M. Baláž, P. Billik, C.Z. Zara, J.M. Criado, F. Delogu, E. Dutková, E. Gaffet, F.J. Gotor, R. Kumar, I. Mitov, T. Rojac, M. Senna, A. Streletskii, W.C. Krystyna, Hallmarks of mechanochemistry: from nanoparticles to technology, Chem. Soc. Rev. 42 (2013) 7571–7637, https://doi.org/10.1039/c3cs35468g.
[51] M.L. Toebes, J.A. Van Dillen, K.P. De Jong, Synthesis of supported palladium catalysts, J. Mol. Catal. Chem. 173 (2001) 75–98, https://doi.org/10.1016/S1381-1169(01)00146-7.
[52] M.C. Biesinger, L.W.M. Lau, A.R. Gerson, R.S.C. Smart, Resolving surface chemical states in XPS analysis of first row transition metals, oxides and hydroxides: Sc, Ti, V, Cu and Zn, Appl. Surf. Sci. 257 (2010) 887–898, https://doi.org/10.1016/j.apsusc.2010.07.086.
[53] K. Murata, D. Kosuge, J. Ohyama, Y. Mahara, Y. Yamamoto, S. Arai, A. Satsuma, Exploiting metal-support interactions to tune the redox properties of supported Pd catalysts for methane combustion, ACS Catal. 10 (2020) 1381–1387, https://doi.org/10.1021/acscatal.9b04524.
[54] S. Capelli, S. Cattaneo, M. Stucchi, A. Villa, L. Prati, Inorganica Chimica Acta Iron as modifier of Pd and Pt-based catalysts for sustainable and green processes, Inorg. Chim. Acta. 535 (2022) 120856, https://doi.org/10.1016/j.ica.2022.120856.
[55] C. Zheng, M. Li, H. Liu, Z. Xu, Complete dehalogenation of bromochloroacetic acid by liquid phase catalytic hydrogenation over Pd/CeO2 catalysts, Chemosphere 239 (2020), 124740, https://doi.org/10.1016/j.chemosphere.2019.124740.
[56] L. Ouyang, P. Tian, G. Da, X. Xu, C. Ao, T. Chen, R. Si, J. Xu, Y. Han, The origin of active sites for direct synthesis of H 2 O 2 on Pd/TiO 2 catalysts : interfaces of Pd and PdO domains, J. Catal. 321 (2015) 70–80, https://doi.org/10.1016/j.jcat.2014.10.003.
[57] L. Dong, Y. Tang, B. Li, L. Zhou, F. Gong, H. He, B. Sun, C. Tang, F. Gao, L. Dong, Influence of molar ratio and calcination temperature on the properties of $Ti_xSn_{1-x}O_2$ supporting copper oxide for CO oxidation, Appl. Catal. B Environ. 180 (2016) 451–462, https://doi.org/10.1016/j.apcatb.2015.06.034.
[58] H. Huang, X. Ye, H. Huang, L. Zhang, D.Y.C. Leung, Mechanistic study on formaldehyde removal over Pd/TiO 2 catalysts : oxygen transfer and role of water vapor, Chem. Eng. J. 230 (2013) 73–79, https://doi.org/10.1016/j.cej.2013.06.035.
[59] S. Lu, F. Wang, C. Chen, F. Huang, K. Li, Catalytic oxidation of formaldehyde over CeO 2 -Co 3 O 4 catalysts, J. Rare Earths 35 (2017) 867–874, https://doi.org/10.1016/S1002-0721(17)60988-8.
[60] L.M. Neal, M.L. Everett, G.B. Hoflund, H.E. Hagelin-Weaver, Characterization of palladium oxide catalysts supported on nanoparticle metal oxides for the oxidative coupling of 4-methylpyridine, J. Mol. Catal. Chem. 335 (2011) 210–221, https://doi.org/10.1016/j.molcata.2010.11.036.
[61] N.S. Babu, N. Lingaiah, N. Pasha, J.V. Kumar, P.S.S. Prasad, Influence of Particle Size and Nature of Pd Species on the Hydrodechlorination of Chloroaromatics : Studies on Pd/TiO 2 Catalysts in Chlorobenzene Conversion, vol. 141, 2009, pp. 120–124, https://doi.org/10.1016/j.cattod.2008.03.018.
[62] V. Bratan, C. Munteanu, C. Hornoiu, A. Vasile, F. Papa, R. State, S. Preda, D. Culita, N.I. Ionescu, Applied Catalysis B : environmental CO oxidation over Pd supported catalysts — in situ study of the electric and catalytic properties, Appl. Catal. B Environ. 207 (2017) 166–173, https://doi.org/10.1016/j.apcatb.2017.02.017.
[63] Z. Karpiński, Catalysis by supported, unsupported, and electron-deficient palladium, Adv. Catal. 37 (1990) 45–100, https://doi.org/10.1016/S0360-0564(08)60363-6.
[64] L.M. Esteves, M.H. Brijaldo, F.B. Passos, Journal of Molecular Catalysis A : chemical Decomposition of acetic acid for hydrogen production over Pd/Al 2 O 3 and Pd/TiO 2 : influence of metal precursor, J. Mol. Catal. Chem. 422 (2016) 275–288, https://doi.org/10.1016/j.molcata.2016.02.001.
[65] D. Fuentes-Perujo, J. Santamaría-González, J. Mérida-Robles, E. Rodríguez-Castellón, A. Jiménez-López, P. Maireles-Torres, R. Moreno-Tost, R. Mariscal, Evaluation of the acid properties of porous zirconium-doped and undoped silica materials, J. Solid State Chem. 179 (2006) 2182–2189, https://doi.org/10.1016/j.jssc.2006.04.018.
[66] Gervasini Antonella, Auroux Aline, Acidity and basicity of metal oxide surfaces 1 II . Determination by catalytic decomposition of isopropanol, J. Catal. 131 (1991) 190–198, https://doi.org/10.1016/0021-9517(91)90335-2.
[67] X. Chen, Y. Shen, S.L. Suib, C.L.O. Young, Catalytic decomposition of 2-propanol over different metal-cation-doped, OMS-2 Mater. 302 (2001) 292–302, https://doi.org/10.1006/jcat.2000.3063.
[68] M.E. Manríquez, T. López, R. Gómez, J. Navarrete, Preparation of TiO 2 – ZrO 2 mixed oxides with controlled acid – basic properties, J. Mol. Catal. Chem. 220 (2004) 229–237, https://doi.org/10.1016/j.molcata.2004.06.003.
[69] L. Collado, P. Reñones, J. Fermoso, F. Fresno, L. Garrido, V. Pérez-Dieste, C. Escudero, M.D. Hernández-Alonso, J.M. Coronado, D.P. Serrano, V.A. de la Peña O'Shea, The role of the surface acidic/basic centers and redox sites on TiO2 in the photocatalytic CO2 reduction, Appl. Catal. B Environ. 303 (2022), https://doi.org/10.1016/j.apcatb.2021.120931, 0–10.
[70] R. Vidruk, M. V Landau, M. Herskowitz, V. Ezersky, A. Goldbourt, Control of surface acidity and catalytic activity of c -Al 2 O 3 by adjusting the nanocrystalline contact interface, J. Catal. 282 (2011) 215–227, https://doi.org/10.1016/j.jcat.2011.06.018.
[71] B. Sudduth, D. Yun, J. Sun, Y. Wang, Facet-Dependent selectivity of CeO2 nanoparticles in 2-Propanol conversion, J. Catal. 404 (2021) 96–108, https://doi.org/10.1016/j.jcat.2021.09.009.
[72] R. Issaadi, C.-E.C. Francois Garin, Study of the acid character of some palladium-modified pillared clay catalysts : use of isopropanol decomposition as test reaction, Catal. Today 113 (2006) 166–173, https://doi.org/10.1016/j.cattod.2005.11.062.
[73] J.N. Díaz de Leon, A. Cruz-Taboada, Y. Esqueda-Barron, G. Alonso-Nuñez, S. Loera-Serna, A.M. Venezia, M.E. Poisot, S. Fuentes-Moyado, Catalytic dehydration of 2 propanol over Al2O3-Ga2O3 and Pd/Al2O3-Ga2O3 catalysts, Catal. Today 356 (2020) 339–348, https://doi.org/10.1016/j.cattod.2019.05.024.
[74] S. Pyen, E. Hong, M. Shin, Y. Suh, C. Shin, Acidity of co-precipitated SiO 2 -ZrO 2 mixed oxides in the acid-catalyzed dehydrations of iso -propanol and formic acid, Mol. Catal. 448 (2018) 71–77, https://doi.org/10.1016/j.mcat.2018.01.031.
[75] D.V. Potapenko, Z. Li, Y. Lou, Y. Guo, R.M. Osgood, 2-Propanol reactivity on in situ prepared Au(1 1 1)-supported TiO 2 nanocrystals, J. Catal. 297 (2013) 281–288, https://doi.org/10.1016/j.jcat.2012.10.020.
[76] S. Feng, K. Takahashi, H. Miura, T. Shishido, One-pot synthesis of lactic acid from glycerol over a Pt/L-Nb2O5 catalyst under base-free conditions, Fuel Process. Technol. 197 (2020), 106202, https://doi.org/10.1016/j.fuproc.2019.106202.
[77] S. Carrettin, P. McMorn, P. Johnston, K. Griffin, G.J. Hutchings, Selective oxidation of glycerol to glyceric acid using a gold catalyst in aqueous sodium hydroxide, Chem. Commun. 7 (2002) 696–697, https://doi.org/10.1039/b201112n.
[78] X. Zhang, M. Gao, P. Yang, X. Cui, Y. Liu, D. Li, J. Feng, Insight into the effect of support crystal form on semi-continuous oxidation of glycerol, J. Porous Mater. 28 (2021) 1371–1385, https://doi.org/10.1007/s10934-021-01088-y.
[79] Z. Yuan, Z. Gao, B.Q. Xu, Acid-base property of the supporting material controls the selectivity of Au catalyst for glycerol oxidation in base-free water, Cuihua Xuebao/Chinese J. Catal. 36 (2015) 1543–1551, https://doi.org/10.1016/S1872-2067(15)60936-6.
[80] N. Dimitratos, J.A. Lopez-Sanchez, D. Lennon, F. Porta, L. Prati, A. Villa, Effect of particle size on monometallic and bimetallic (Au,Pd)/C on the liquid phase oxidation of glycerol, Catal. Lett. 108 (2006) 147–153, https://doi.org/10.1007/s10562-006-0036-8.
[81] M.R.A. Arcanjo, I.J. Silva, E. Rodríguez-Castellón, A. Infantes-Molina, R.S. Vieira, Conversion of glycerol into lactic acid using Pd or Pt supported on carbon as catalyst, Catal. Today 279 (2017) 317–326, https://doi.org/10.1016/j.cattod.2016.02.015.
[82] M. Hosseini, S. Siffert, H.L. Tidahy, R. Cousin, J.F. Lamonier, A. Aboukais, A. Vantomme, M. Roussel, B.L. Su, Promotional effect of gold added to palladium supported on a new mesoporous TiO2 for total oxidation of volatile organic compounds, Catal. Today 122 (2007) 391–396, https://doi.org/10.1016/j.cattod.2007.03.012.
[83] E. Skrzyńska, A. Wondołowska-Grabowska, M. Capron, F. Dumeignil, Crude glycerol as a raw material for the liquid phase oxidation reaction, Appl. Catal. Gen. 482 (2014) 245–257, https://doi.org/10.1016/j.apcata.2014.06.005.
[84] M.R.A. Arcanjo, M. Paniagua, G. Morales, J. Iglesias, J. Melero, R.S. Vieira, I. Silva, E. Rodr, Temperature E Ff Ect on Pretreatment of the Activated Carbon Support (Pt/AC and Pd/AC) for Glycerin into Lactic Acid, 2020, https://doi.org/10.1021/acs.iecr.0c01588.